Design and characterization of a broadband PCB-based coaxial sensor for permittivity screening in skin cancer detection applications

Mohamed Zied Fritiss, Patrick Poulichet, Hakim Takhedmit, Laurent Lanquetin, Stephane Protat, Patrice Vallade, Elodie RICHALOT, Olivier Français

Design and characterization of a broadband PCB-based coaxial sensor for permittivity screening in skin cancer detection applications

Mohamed Zied Fritiss[1,2], Patrick Poulichet[1], Hakim Takhedmit[1], Laurent Lanquetin[2], Stephane Protat[1], Patrice Vallade[1], Elodie Richalot[1], Olivier Français[1]
[1] ESYCOM, CNRS UMR 9007, Université Gustave Eiffel. F-77454 Marne-la-Vallée, France
[2] Segula Technologies, pôle d'activité Pissaloup, 8 Av. Jean d'Alembert, 78190 Trappes France

E-mail : zied.fritiss@segula.fr

Received xxxxxx
Accepted for publication xxxxxx
Published xxxxxx

Abstract

Broadband dielectric spectroscopy is nowadays considered as a useful non-destructive detection tool for biomedical applications like glucose monitoring, hydration level measurement, and cancer tissue examination. Depending on their composition and physiological state, biological tissues have different dielectric characteristics. Studies on melanoma have revealed that the lesion site's skin permittivity changes depending on the malignancy of the lesion. In that case, the complex permittivity of suspicious areas must therefore be imaged with spatial resolution consistent with the small dimensions of the pathology in order to correctly detect and characterize the lesion site. The variety of skin properties for various individuals and physiological situations (such as temperature and humidity), however, makes it difficult to build a sensitive sensor capable of detecting minor fluctuations in permittivity in every situation. In order to detect suspicious lesions in their early stage with a good agreement between simulated and measured results, this work proposes the design of a unique microwave sensor that can precisely detect small variations in cutaneous permittivity between 1 and 6 GHz.

Keywords: RF sensor; dielectric properties; biological tissues; non-destructive pre-diagnosis; cancer tissue analysis; melanoma; cutaneous permittivity; early tumor detection.

1. INTRODUCTION

Biological tissue dielectric characteristics differ depending on their constitution and the person's physiological conditions. In particular, it has been shown that the dielectric properties vary between a healthy tissue and a tumor in the case of different cancers [1]. In the case of cutaneous melanoma, with regard to the significant water content of the malignant cells, a tumor is characterized by a skin permittivity variation at the site of the lesion [2]. This makes reflectometry an interesting non-invasive tool for skin cancer detection [3]. A significant obstacle is to develop a wideband RF sensor that can capture the complex permittivity of a suspicious area with an appropriate spatial resolution compared to the small size of the region of interest (an average diameter of 6 mm) [4]. In fact, the sensitivity needed to detect fine permittivity alterations in order to accurately discriminate the type and stage of the lesion presents a challenge in the design and optimization of such a sensor. Skin sensors operating over different frequency ranges have been proposed. Measurements at 300MHz suffer from the moderate permittivity contrast between skin states [5] and a sensitive area surface larger than the previously

mentioned size of interest. As a frequency increase permits a reduction of the sensitive area surface, reflectometry tools in the Ka-band [6] [7] and above [8] [9] are reported. Besides, a commercial skin cancer detection tool based on impedance spectroscopy in the 1 KHz – 2.5 MHz frequency band has been presented in [10]. A low-cost solution is proposed in this paper with measurements performed over a lower frequency band on which the permittivity differences between normal skin and different lesion types are important; indeed, the permittivity variation is noticeable between different types of lesions in the 1 GHz - 14 GHz frequency band according to the measurement results presented in [11]. Considering RF sensors, the open-ended coaxial probe is one of the most popular. It has many benefits, including simplicity in design and execution as well as excellent resolution [12]. It has been shown that coaxial probes can be used to extract the skin permittivity by reflectometry in the 0.3 - 6GHz frequency band and permits to distinguish normal skin from a lesion [3]. The reduction of the probe diameter allows to examine small surfaces while keeping good measurement accuracy [13]. The use of SIW (Substrate Integrated Waveguide) technology in the context of melanoma detection, as proposed in this paper, enables considering the sensor integration on a substrate, with millimeter-scale dimensions, opening the way to further development prospects [14]. In order to consider the early detection of various forms of tumor, this paper presents the results of a sensitive and innovative RF sensor that can accurately identify small fluctuations in skin permittivity over a wide frequency band.

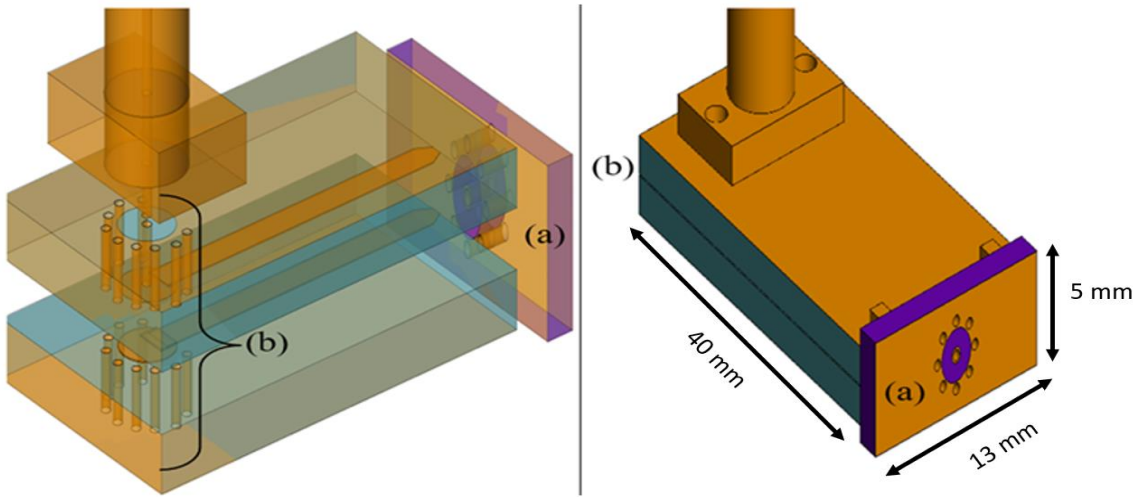

Figure 1: *3D view of the different elements of the proposed probe: (a) open-ended sensitive area, (b) SMA connector to stripline transition.*

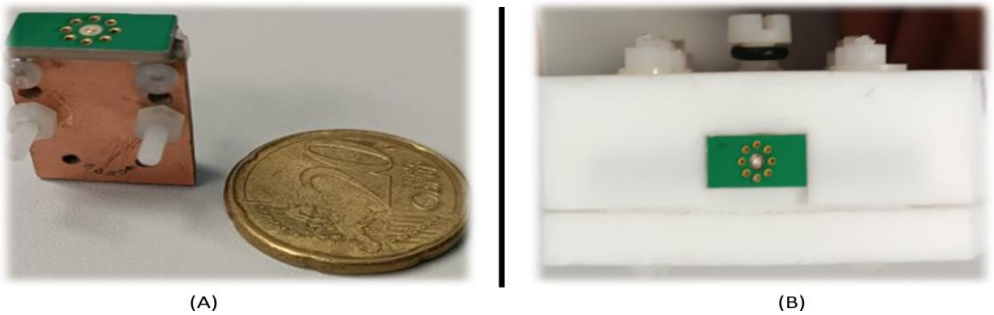

Figure 2: *The first prototype unboxed view (A) and the boxed view (B)*

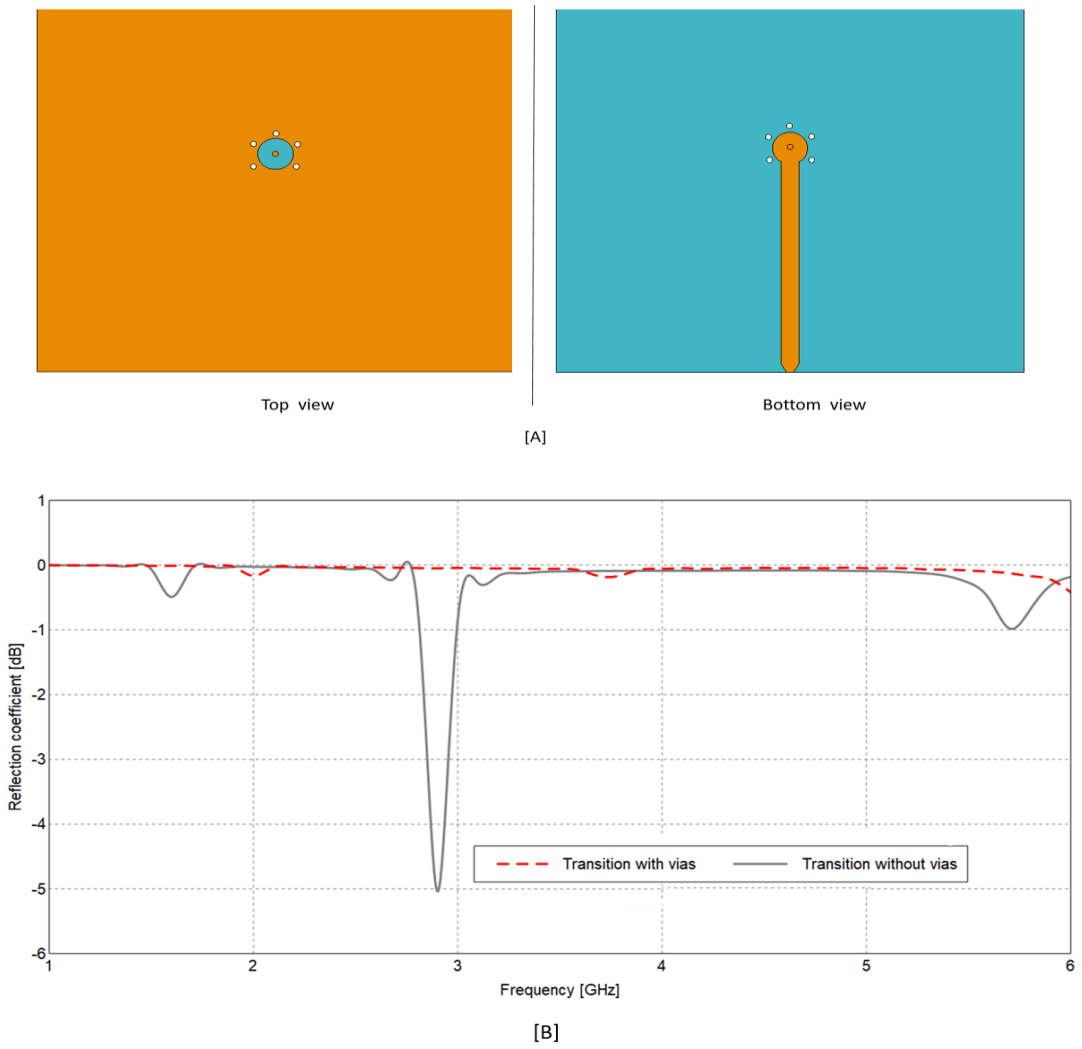

Figure 3: *Stripline optimisation: Top/Bottom views (A) and the impact of metallized vias on the connector/line transition (S_{11} comparison) (B)*

2. MATERIAL AND METHODS

2.1 Design and optimization of the sensor

The RF sensor is composed of two parts: i) a strip-line for signal transmission from an SMA connector to the sensitive part and ii) a miniature measurement region mimicking a coaxial open-ended probe. The sensitive component is printed on a Rogers 3003 substrate (ε_r = 3 @10 GHz, tan δ= 0.0010) with a central metallized via hole to serve as the coaxial line center core (Figure 1. a). A metallic wall is created by the circular arrangement of metallized vias surrounding the central conductor. Two Arlon 25N (ε_r = 3.32 @10 GHz, tan δ= 0.0025) substrates form the strip line (Figure 1. b), while they are stacked and linked together to assure a good contact. For measurement, a specific packaging (based on a homemade Teflon box (Figure 2.B)) ensures good contact between the two Arlon 25N substrates to prevent liquid infiltration and decrease the air gap between them.

The sensitive part (Figure 4) is printed on a 1.52 mm thick Roger 3003 substrate. A 0.5 mm diameter metallized via is used as a central conductor at the center of a 2.3 mm diameter circular area where the metallization is removed. Metallized vias of 0.5 mm diameter are also used as the outer conductor assuring a better resolution (Figure 5).

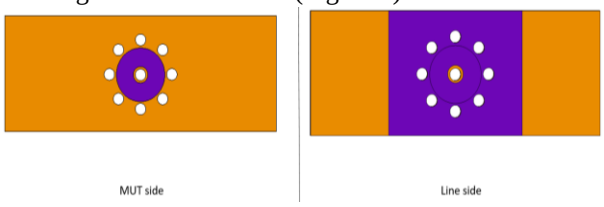

Figure 4: *Line and MUT sides of the sensitive part*

2.2 Simulation and optimization of the stripline

The 3D simulations have been performed based on the FEM method using FEKO software from which the reflection coefficient (S_{11}) is extracted from 1 GHz to 6 GHz. The 1.53

Materials	ε_s	ε_∞	ε_h	τ_1 (ps)	τ_2 (ps)
Water	78.8	3.3	/	7.37	/
Ethanol	25.2	4.68	/	143.18	/
DMSO	45.19	5.984	/	10.07	/
Skin [16]	33.890	4.489	4.460	3.930	0.488
Tumor [16]	58.371	4.343	4.622	4.983	0.488

Table 1: *Debye parameters of the models used in this paper*

mm wide stripline between two Arlon 25N substrates of 1.524 mm thickness each presents an impedance of 50 Ω and has a length of 40 mm. It is connected to the SMA central core through a 0.5 mm diameter metallized dug at the center of a 2.3 mm diameter circular area where the top metallization is removed to avoid any short-circuit (Figure 3.A). To improve the transmission between the SMA connector and the strip line and avoid the appearance of unwanted resonances, five metallized vias of diameter 0.5 mm have been added around the transition area. The effect of these surrounding vias is shown by the comparison of the simulated reflection coefficients of the unloaded sensor with and without them as shown in Figure 3.B. Frequency fluctuations are observed without vias which would have a harmful effect on the sensor sensitivity. The vias surrounding the transition act like a shield confining the wave thus removing the unwanted resonances from the measurements.

At the end of the stripline, over the last 0.5 mm, the strip width is gradually reduced from 1.53 mm to 0.6 mm to improve the signal transmission to the sensitive part of the sensor (Figure 3.A).

2.3 Extraction method

The complex permittivity ε_r^* of the material under test is extracted from the simulated S_{11} parameter using the following relationship [15]:

$$\varepsilon_r^* = \frac{C_1 S_{11} - C_2}{C_3 + S_{11}} \quad (1)$$

Where C_1, C_2, and C_3 are probe-specific constants that are determined, during the specific calibration step, from the simulated S_{11} obtained for reference materials of known permittivity (de-ionized water, air, ethanol). For a better extraction of the complex parameters, the probed reference materials are in the permittivity range of the calibration materials (ε_r' between 1 and 80). After this calibration step, the complex permittivity of the probed material is deduced from the simulated or measured reflection coefficient S_{11}.

2.4 Skin/tumor phantom tissues synthesis

To properly characterize and experimentally validate the proposed sensor, it is necessary to perform tests close to in vivo measurements. The most widely used method is based on phantom tissues, which have electromagnetic properties close to those of human biological tissues. Thus, phantom tissues have been fabricated to reproduce the dielectric properties of healthy skin and melanoma tumors using non-toxic and biodegradable materials such as gelatin, agar-agar, water, and polyethylene microbeads according to the process described in [17]. For the healthy skin phantom, the same approach as in [18] was followed to mimic the skin properties presented in [16]. Concerning the melanoma tumor phantom, the dielectric properties of sample S6 of [16] have been reproduced by using different materials; indeed, the component proportions were adjusted thanks to the Bruggeman mixing rule to reach the aimed real permittivity without controlling the imaginary part of the relative permittivity with this formula:

$$(V)\frac{\varepsilon_w - \varepsilon_{ef}}{\varepsilon_w + 2\varepsilon_{eff}} + (1-V)\frac{\varepsilon_{pe} - \varepsilon_{eff}}{\varepsilon_{pe} + 2\varepsilon_{eff}} = 0 \quad (2)$$

Where V is the water volumetric ratio, ε_w is the deionized water permittivity, ε_{pe} is the Polyethylene (PE) powder permittivity (that is 2.3), and ε_{eff} the aimed permittivity[19]. Since the tumor phantom was synthesized using PE powder and water instead of the materials used in [16], only the real part of the permittivity is expected to be close to the aimed one, so that the imaginary parts are not presented. Table 1 shows the Debye parameters of the permittivity models used in simulations and considered as references in measurements. To test the probe's ability to detect the permittivity variation, a gradient of polyethylene powder quantity was carried out: an initial quantity of 10 g (15% of the total volume) was used as starting case, then a quantity of 10 g of polyethylene powder was added progressively modifying thus the obtained permittivity until reaching a maximum quantity of 40 g for a minimum theoretical permittivity of 24 (above 40 g various undesirable chemical reactions are observed).

3. RESULTS AND DISCUSSION

3.1 Extracted results

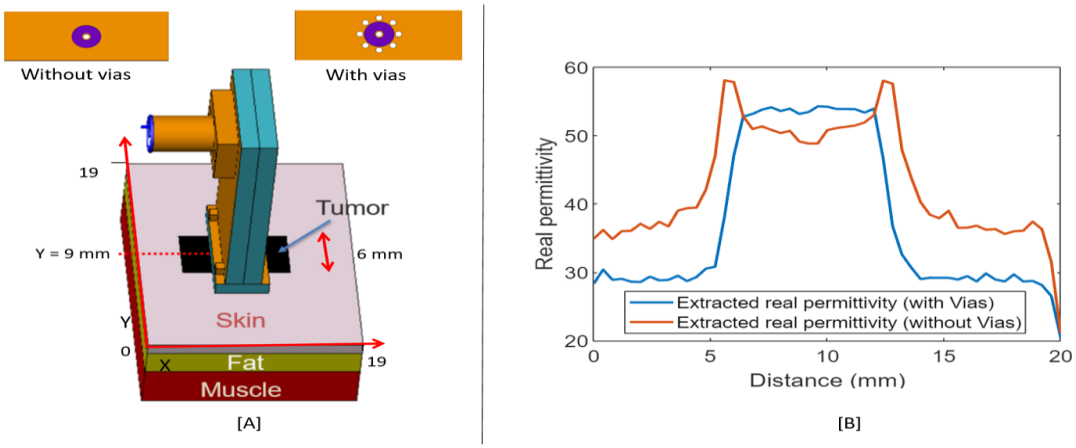

Figure 5: *Simulation results for the probe on a multilayered biological tissue model around the sensitive area, 3D models [A], and extracted real permittivity @3 GHz with and without vias (scanning along x-axis for y = 9 mm) [B]*

The S_{11} parameters obtained from the simulations of various material models are then compared to their relative Debye relaxation models using the relationship (1). Indeed, several skin and tumor models are presented in this paper and the ones corresponding to samples S5 and S6 from [16] have been chosen as skin and tumor models. It can be seen that the difference obtained (Figure 6) is quite small, around 1 % for the skin and tumor complex permittivities compared to the associated Debye relaxation models.

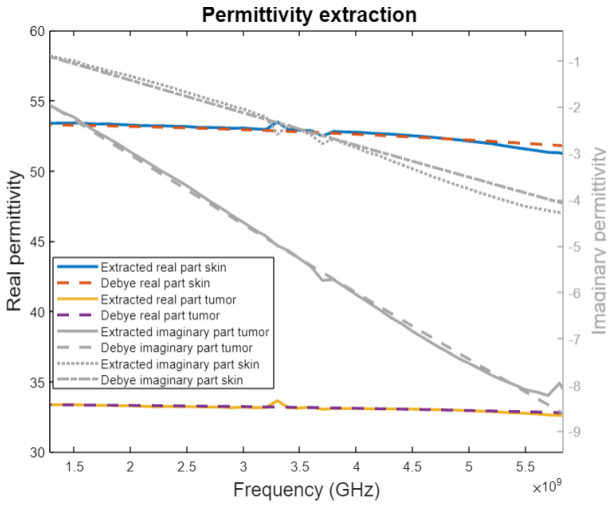

Figure 6: *Extracted skin and tumor model complex permittivity from the simulation results*

Different scenarios were simulated, such as the measurement on a multilayer medium (skin, fat, muscle) or the detection of the position of the tumor (6x6 mm²) in a wide biological multilayered medium (19x19 mm²), by scanning along the x-axis for y = 9 mm (Figure 5). One can notice that the probe correctly detects the permittivity variation when passing by the tumor. In addition, when the sensitive part is not restricted by the metallic vias, the EM waves are less confined which leads to poor performances, whereas a better resolution can be observed and a more accurate variation detection is obtained when using the metallic vias in contrast. The ability of the probe to correctly differentiate different tumor cases was simulated by measuring the real permittivity of multilayered structures (Skin of 1.5 mm, fat of 3 mm, muscle of 5 mm) for a tumor thickness varying from 0.1 mm to 1.5 mm (Figure 7). As a result, the permittivity extracted gradually raises from 45 (thickness of the tumor = 0.1 mm/skin = 1.4 mm) to 60 (thickness of the tumor = 0.5 mm / skin = 1 mm). To characterize the probe resolution, a circular tumor model with a varying diameter was implemented in the center of a skin block of 4 mm side. Figure 8 shows the extracted permitivity from an 4 mm y-axis sweep when the diameter of the tumor D positioned at y = 2 mm is gradually reduced from 2 mm to 0.5 mm. The probe is able to correctly detect a tumor model down to 0.7 mm diameter which is a lot smaller than the average size of a melanoma around 6 mm. This confirms the ability of the probe to follow the tumor evolution and correctly detect the tumor model permittivity when its thickness is at least 0.5 mm. These simulation results show the ability of this innovative RF probe to correctly identify a tumor location and follow its growth.

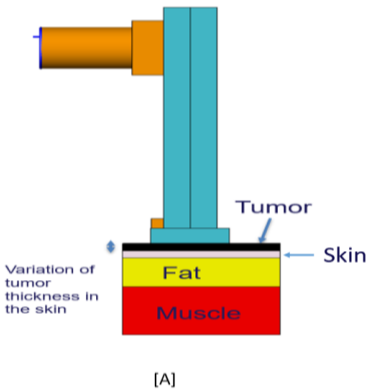

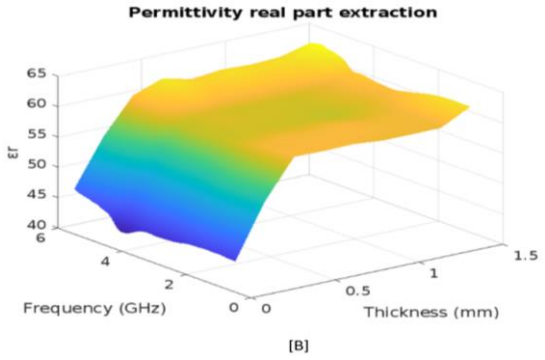

Figure 7: *Simulation results for the probe on a multilayered biological tissue model, 3D models side view [A], and extracted real permittivity for different tumor thicknesses [B]*

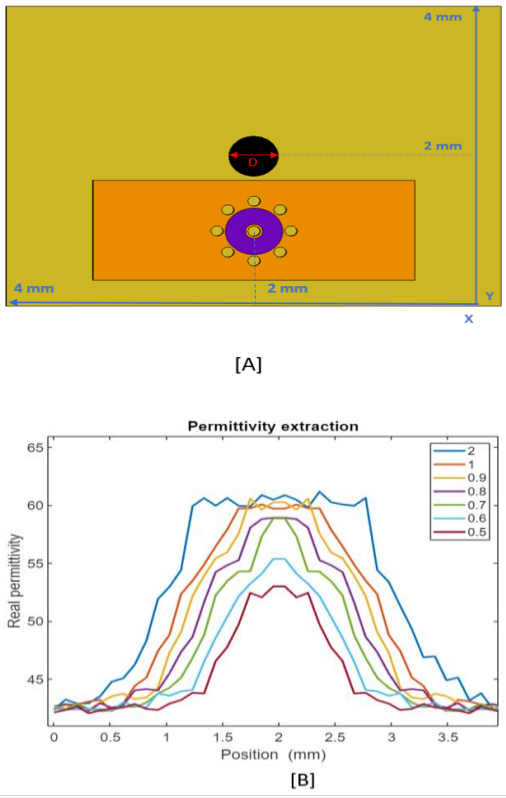

Figure 8: *Simulation results for the probe resolution on a skin/tumor model around the sensitive area, 3D models [A], and extracted real permittivity @3 GHz (scanning along y-axis for x = 2 mm) [B]*

3.2 Sensor optimization (Teflon box)

Considering the first measurements with the probe, the appearance of some unwanted resonances was observed that was not expected from the simulation results. An optimization step has been done to cancel it (Figure 9). These resonances were related to a small air gap inducing a missing contact between the two lines on each Arlon 25N substrates as well as leakage through this air gap during liquid measurements. This phenomenon affects the calibration process by altering the substrate properties. The proposed solution to solve this problem was to put the device inside a Teflon box, in order to apply constant pressure, maintain good contact between the transmission lines, and limit the liquids leaking between the substrates. This packaging gives after permittivity extraction much clearer and stable values (Figure 10).

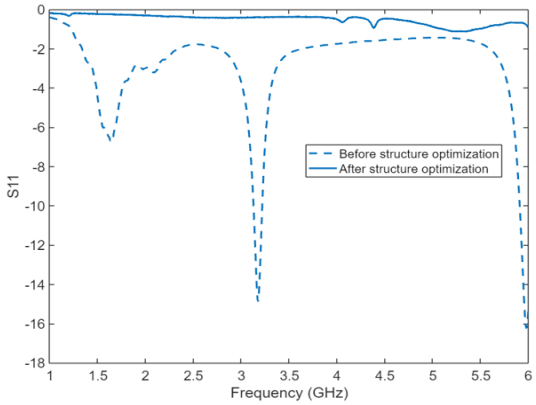

Figure 9: *Measured reflection coefficient for the device before and after its optimization through the packaging. The sensitive area is in vacuum in this case.*

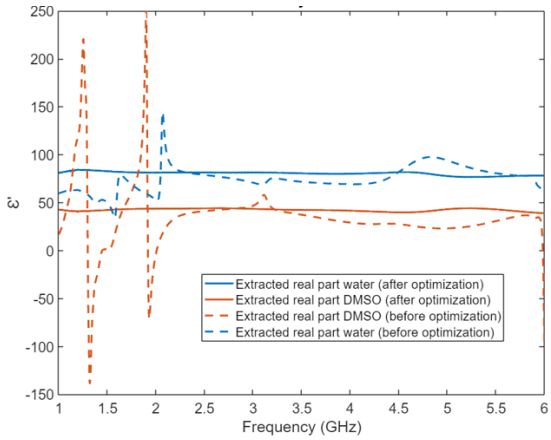

Figure 10: *Permittivity real part extracted from liquids before and after the optimization through the packaging.*

3.3 Measurement results

Measurements of the reflection coefficient (S_{11}) from 1 to 6 GHz on reference media (water, ethanol, and air) and phantom tissues (skin or tumor) were carried out using our sensor (Figure 11) in order to compare the measurements and evaluate the discrimination of the media by the probe. The complex permittivity of the liquids is extracted and compared to the expected values (Figure 12). The small deviations in the extracted permittivity are due to a manufacturing issue and imprecision in the extraction method, causing a small resonance due to the Teflon box. The results obtained through the PE (Polyethylene) powder variation (Figure 13) show that

our sensor has the ability to correctly identify a variation of permittivity.

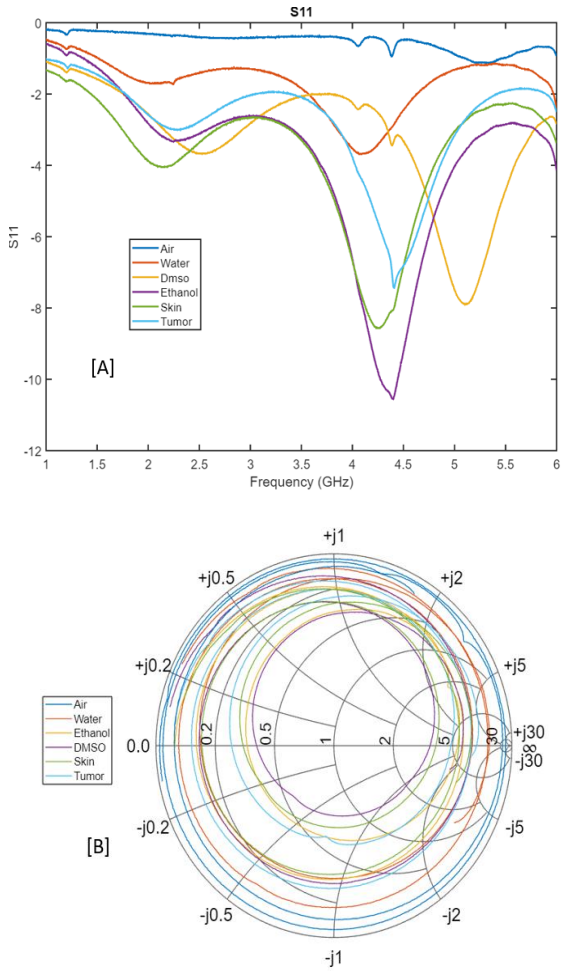

Figure 11: *Measured reflection coefficient for different materials (A) Amplitude in dB (B) Smith chart*

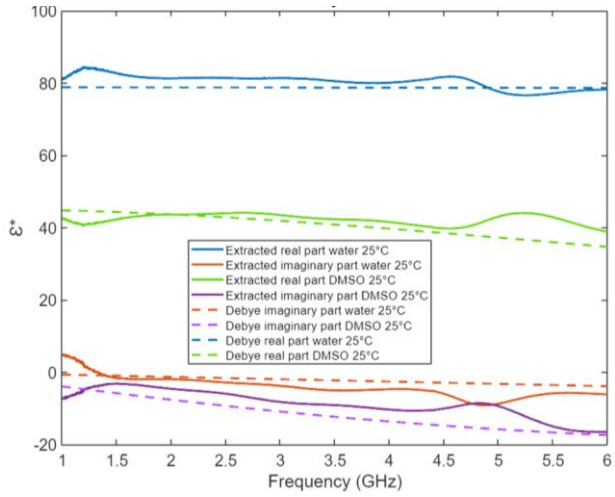

Figure 12: *Permittivity real/imaginary part extracted from measurements for liquids at 25°c*

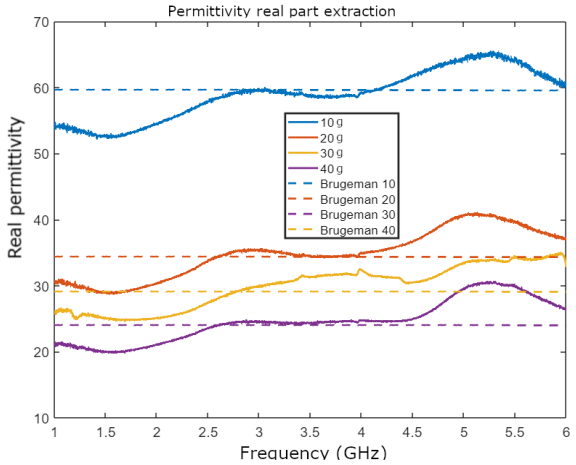

Figure 13: *Permittivity real part extracted from measurement of PE powder based phantom tissue with a variation in PE quantity*

3.4 Differential approach

In order to show the ability of our sensor to differentiate several skin and tumor types, several cases of skin tumors have been studied and simulated [16]. A differential S_{11} approach is proposed to discriminate the different stages of melanoma development with different types of normal skin. The difference ΔS_{11} between the complex reflection parameters obtained for two normal skin (skin1/skin2) and malignant skin models (Skin/tumor model) is represented in Figure 14.

Using this method, the approach consists of comparing the complex reflection coefficients obtained when the probe is placed on safe skin then on a suspiceous region. Whereas in [8] only the amplitude of the reflection coefficients are considered, here variations in its amplitude and phase are used for a better detection of small permittivity variations. The differentiation between normal and malignant skin models is obtained, as the difference ΔS_{11} between the reflection coefficients for two normal skins is around -40 dB, whereas it stays above -20 dB between normal and malignant tissues.

The permittivity extracted from measurements presented in Figure 13 shows that the 10 g PE powder phantom tissue is associated with the real permittivity the closest to one of the tumor models. This phantom tissue is used as a reference for the sensor and measurement analysis. This is the case for the differential method in Figure 15 where 10 g PE powder phantom is the reference and 20/30/40 g PE powder phantoms are the tested materials. As expected, the smallest permittivity difference is associated to the lowest ΔS_{11} values. For the different phantoms of gradually varying PE powder content, ΔS_{11} gradually raises by approximately 2 dB for every 10g of

PE added which can be interpreted as a variation of 5 for the real part of the permittivity.

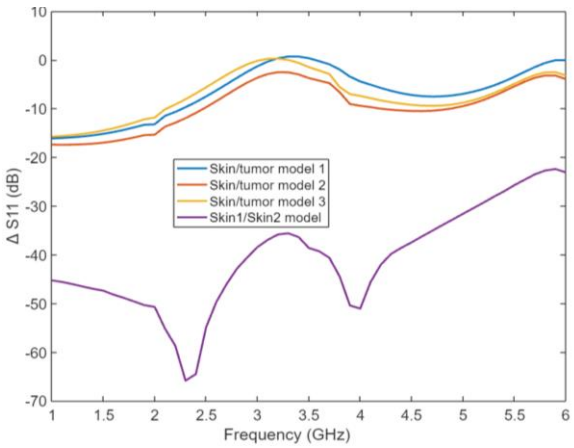

Figure 14: *Simulation results for differential method using models from [15]*

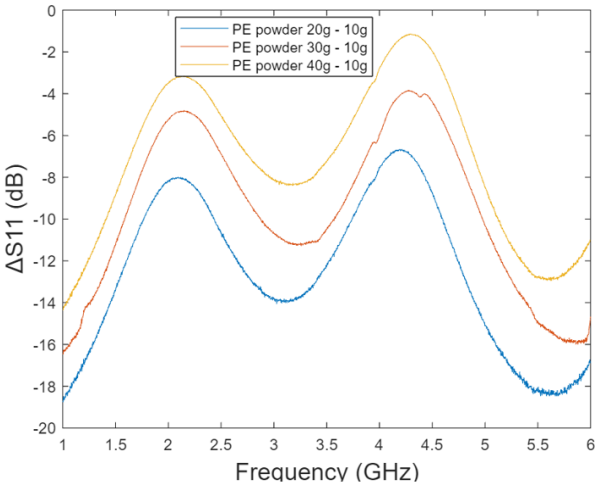

Figure 15: *Measurement results for differential method with PE powder-based phantoms*

3.5 Discussion on the probe specifications

The proposed probe specifications were compared to other coaxial probes used with the same objective of identifying skin lesions (See Table 2). By considering the data, our probe is in a good position and fits well with the goal considering also the resolution. It highlights some advantages of the approach presented in this paper : i) the planar technology (based on PCB) allows easy link to other RF devices with a low cost sensor, ii) as seen in [11], the frequency range used is well suited for skin/melanoma differentiation due to the clear permittivity difference and is easily accessible with most commercial Vector Network Analysers (VNA), iii) the differential method permits to avoid the calibration step using reference materials and thus makes this tool easier to use for medical practitioners.

Reference	Sensitive surface dimensions	Frequency range	Technology
[3]	Diameter 3.62 mm	0.3 GHz - 6 GHz	Open-ended coaxial probe
[5]	Diameter 9mm	300 MHz	Integrated open-ended coaxial probe
[6]	3.556mm x 7.112mm	26.5GHz – 40GHz	Open-ended rectangular waveguide
[7]	0.64mm x 2.3mm	35GHz – 45GHz	Substrate integrated waveguide
[8]	tip size of 0.6 mm x (0.3 mm to 1.0 mm)	90GHz - 104 GHz	Tapered dielectric rod waveguide
[9]	0.35mm x 0.7mm	90GHz – 150GHz	Dielectric filled Rectangular waveguide
[13]	Diameters 0.5mm, 0.9mm and 2.2mm	0.5 GHz - 6 GHz	Open-ended coaxial probe
[20]	Diameter 1.8mm and 2mm	10 MHz - 3 GHz	Open-ended coaxial probe
[21]	Diameter 3.5mm	200MHz - 50GHz	Open-ended coaxial probe
[22]	1.6mm x 3mm	Up to 6 GHz	Microstrip line
[23]	Diameter 2.2mm	1GHz - 30 GHz	Keysight open-ended coaxial Slim probe
[24]	About 5 mm of diameter	Up to 5GHz	Planar probe acting as an open-ended coaxial probe
This work	Diameter 2.3mm	1GHz - 6GHz	PCB-based coaxial probe

Table 2: *State of the art comparison*

4. CONCLUSION

These first results presented on an innovative PCB-based RF sensor make it possible to validate its ability to analyze tissues in the RF band, from 1 to 6 GHz. The sensor can be considered in order to discriminate a tumor from a healthy tissue while maintaining a small sensing surface (current detection area of 2.8 mm diameter with a 0.7 mm resolution), with the ability to differentiate normal skin from tumor models by extracting the complex reflection coefficient S_{11}.

Based on 3D RF simulation analysis, dielectric properties of small skin tumor, taking into account multilayered tissue (skin, fat, tumor), have been extracted. Results show the feasibility of detecting and monitoring a small skin tumor ($0.7*0.7$ mm^2). Phantom tissues have been developed and used to mimic tumor dielectric properties for testing. A good correlation between simulation and measurement confirms the performance of the RF sensor.

An original differential method, to simplify the measurement steps by removing the calibration process, was tested. This approach permits the discrimination of healthy skin from a tumor using simulation and measurement on dedicated phantom tissues (with a difference indicator of -40 dB between skin/skin models against values between -15 and 0 dB between skin/tumor models).

This new proposed PCB-based RF sensor offers new opportunities for the dielectric analysis of biological materials and in particular in the case of early-stage cancerous skin tissues analysis.

References

[1] Heba Mohamed Fahmy, Amany Mohamed Hamad, Fatma Al-zahraa Sayed, Youssef S. Abdelaziz, Esraa Samy Abu Serea, Amany Bahaa El-Din Mustafa, Maha Amir Mohammed, Ayat M. Saadeldin, “Dielectric spectroscopy signature for cancer diagnosis: A review”, Microwave and Optical Technology Letters, December 2020.

[2] Mirbeik-Sabzevari, Amir, Robin Ashinoff, and Negar Tavassolian. "Ultra-wideband millimeter-wave dielectric characteristics of freshly excised normal and malignant human skin tissues." IEEE Transactions on Biomedical Engineering 65.6 (2017): 1320-1329.

[3] P. Mehta, K. Chand, D. Narayanswamy, D. G. Beetner, R. Zoughi and W. V. Stoecker, "Microwave reflectometry as a novel diagnostic tool for detection of skin cancers," in IEEE Transactions on Instrumentation and Measurement, vol. 55, no. 4, pp. 1309-1316, Aug. 2006, doi: 10.1109/TIM.2006.876566.

[4] B. J. Mohammed, S. A. R. Naqvi, M. Manoufali, K. Bialkowski, A. M. Abbosh, "Changes in epidermal dielectric properties due to skin cancer across the band 1 to 50 GHz." 2018 Australian Microwave Symposium (AMS). IEEE, 2018.

[5] Mayrovitz, HN, Gildenberg, SR, Spagna, P, Killpack, L, Altman, DA. “Characterizing the tissue dielectric constant of skin basal cell cancer lesions.” Skin Res Technol. 2018; 24: 686– 691. https://doi.org/10.1111/srt.12585

[6] Y. Gao, M. T. Ghasr, M. Nacy and R. Zoughi, "Towards Accurate and Wideband In Vivo Measurement of Skin Dielectric Properties," in IEEE Transactions on Instrumentation and Measurement, vol. 68, no. 2, pp. 512-524, Feb. 2019, doi: 10.1109/TIM.2018.2849519.

[7] Giulia Mansutti, Ahmed Toaha Mobashsher, Amin Abbosh, “Design of a Millimeter-Wave Near-Field Probe for Early-Stage Skin Cancer Detection”, 13th European Conference on Antennas and Propagation (EuCAP 2019) Réécrire correctement cette reference

[8] F. Töpfer, S. Dudorov and J. Oberhammer, "Millimeter-Wave Near-Field Probe Designed for High-Resolution Skin Cancer Diagnosis," in IEEE Transactions on Microwave Theory and Techniques, vol. 63, no. 6, pp. 2050-2059, June 2015, doi: 10.1109/TMTT.2015.2428243.

[9] K. Y. Chan and R. Ramer, "Millimetre-wave near field probe for skin defects detection," 2015 International Conference on Electromagnetics in Advanced Applications (ICEAA), Turin, Italy, 2015, pp. 1392-1395, doi: 10.1109/ICEAA.2015.7297346.

[10] Sarac, Esra et al. “Diagnostic Accuracy of Electrical Impedance Spectroscopy in Non-melanoma Skin Cancer.” Acta dermato-venereologica vol. 100,18 adv00328. 23 Nov. 2020, doi:10.2340/00015555-3689

[11] S. A. R. Naqvi, A. T. Mobashsher, B. Mohammed, D. Foong and A. Abbosh, "Benign and Malignant Skin Lesions: Dielectric Characterization, Modelling and Analysis in Frequency Band 1 to 14 GHz," in IEEE Transactions on Biomedical Engineering, vol. 70, no. 2, pp. 628-639, Feb. 2023, doi: 10.1109/TBME.2022.3199094.

[12] La Gioia, E. Porter, I. Merunka, A. Shahzad, A. Salahuddin, M. Jones, & M. O’Halloran "Open-ended coaxial probe technique for dielectric measurement of biological tissues: Challenges and common practices." Diagnostics 8.2 (2018): 40.

[13] C. Aydinalp, S. Joof, T. Yilmaz, N. P. Özsobaci, F. A. Alkan and I. Akduman, "In Vitro Dielectric Properties of Rat Skin Tissue for Microwave Skin Cancer Detection," 2019 International Applied Computational Electromagnetics Society Symposium (ACES), Miami, FL, USA, 2019, pp. 1-2.

[14] Paul M. Meaney, Shireen D. Geimer, Robin Augustine, Keith D. Paulsen,” Quasi- Open-Ended Coaxial Dielectric Probe Array for Skin Burn Characterization”, 13th European Conference on Antennas and Propagation (EuCAP 2019)

[15] Norman Wagner, Moritz Schwing, Alexander Scheuerman," Numerical 3-D FEM and Experimental Analysis of the Open-Ended Coaxial Line Technique for Microwave Dielectric Spectroscopy on Soil" IEEE Transactions on Geoscience and Remote Sensing, 2013, vol. 52, no. 2, O. 880-893.

[16] Zhang, R., Yang, K., Yang, B. et al. Dielectric and "Double Debye Parameters of Artificial Normal Skin and Melanoma. " J Infrared Milli Terahz Waves 40, 657–672 (2019). https://doi.org/10.1007/s10762-019-00597-x

[17] R. Aminzadeh, M. Saviz, and A. A. Shishegar, "Characterization of low-cost tissue mimicking materials at millimeter-wave frequencies," 2015 23rd Iranian Conference on Electrical Engineering, 2015, pp. 283-287, doi: 10.1109/IranianCEE.2015.7146225.

[18]Aminzadeh, R., Saviz, M. and Shishegar, A.A. ,"Theoretical and experimental broadband tissue-equivalent phantoms at microwave and millimetre-wave frequencies. " Electron.Lett. (2014),50: 618-620. https://doi.org/10.1049/el.2014.0749

[19] S. Gabriel, R. W. Lau, and C. Gabriel, "The dielectric properties of biological tissues: III. Parametric models for the dielectric spectrum of tissues," Phys. Med. Biol., vol. 41, 1996.

[20]E.Canicattì, N.Fontana, S.Barmada and A.Monorchio, "Dielectric Characterization Improvement of Biopsy Samples Via a Coated Open-Ended Coaxial Probe," 2022 Microwave Mediterranean Symposium (MMS), Pizzo Calabro, Italy, 2022, pp. 1-4, doi: 10.1109/MMS55062.2022.9825517.

[21] Keysight," Dielectric Probe Kit 200 MHz to 50 GHz, high temperature probe", Keysight 85070E, December 2, 2017

[22] David Dubuc, Katia Grenier, Florent Morfoisse, Barbara Susini-Garmy. "In vitro and in vivo investigations toward near-field microwave-based detection of melanoma. " IEEE International Microwave Bio Conference 2017, May 2017, Goteborg, Sweden. 4p. hal-01529825.

[23] Syed Akbar Raza Naqvi , Mohamed Manoufali , Beadaa Mohammed , Ahmed Toaha Mobashsher , Damien Foong , and Amin M. Abbosh, "In Vivo Human Skin Dielectric Properties Characterization and Statistical Analysis at Frequencies From 1 to 30 GHz", IEEE TRANSACTIONS ON INSTRUMENTATION AND MEASUREMENT, VOL. 70, 2021

[24] P.M. Meaney, T. Zhou, A. Borsic, T. Farkas "Planar Probe and system for measuring dielectric properties of biological materials." U.S. Patent No. 9, 880,118. 30 Jan. 2018.